

# Adsorption of Rhodamine B from water by activated char obtained from end-of-life tyre pyrolysis

Krzysztof Kuśmierek<sup>1</sup> , Andrzej Świątkowski<sup>1</sup> , Tomasz Kotkowski<sup>2</sup> , Robert Cherbański<sup>2\*</sup> ,  
Eugeniusz Molga<sup>2</sup> 

<sup>1</sup> Military University of Technology, Faculty of Advanced Technologies and Chemistry, ul. Kaliskiego 2, 00-908 Warsaw, Poland

<sup>2</sup> Warsaw University of Technology, Faculty of Chemical and Process Engineering, ul. Waryńskiego 1, 00-645 Warsaw, Poland

## Abstract

Three activated chars obtained from end-of-life tyre pyrolysis differing in activation time (AC110 – 110 min, AC130 – 130 min, and AC150 – 150 min) were successfully used as adsorbents for the removal of model dye – Rhodamine B (RhB) from aqueous solutions. The effects of solution pH, adsorption kinetics, and equilibrium adsorption were investigated. The results showed that the adsorption was strongly pH-dependent; the highest percentage of RhB dye adsorbed was obtained at pH 2.0 and the removal efficiency decreased with an increase in solution pH. Adsorption kinetics was analyzed using pseudo-first-order, pseudo-second-order, Weber-Morris, and Boyd kinetic models. It was found that the pseudo-second-order kinetic equation was the most appropriate for describing the adsorption kinetics and that the RhB adsorption process was controlled by a film diffusion mechanism. Adsorption equilibrium data were fitted to the Langmuir, Freundlich, Temkin, and Elovich isotherm models. The equilibrium data were best represented by the Langmuir model with the monolayer adsorption capacities of 69.96, 94.34, and 133.3  $\mu\text{mol/g}$  for AC110, AC130, and AC150, respectively. It was concluded that the adsorption of RhB was closely correlated with the specific surface area (and activation time) of the activated chars.

## \* Corresponding author:

e-mail:

[robert.cherbanski@pw.edu.pl](mailto:robert.cherbanski@pw.edu.pl)

## Article info:

Received: 24 June 2022

Revised: 02 November 2022

Accepted: 14 December 2022

## Keywords

Rhodamine B, adsorption, pyrolysis, waste tyres, tyre pyrolysis char

## 1. INTRODUCTION

New data on end-of-life tyre (ELT) management from the European Tyre and Rubber Manufacturers' Association shows that 95% of the arising ELTs were collected and treated in the EU27 and UK in 2019 (ETRMA, 2021). On the other hand, the percentage of those treated in Poland is much lower than the European average and amounts only to 79%. The rest of the ELTs (21%) are either stocked, their fate is unknown or still awaiting treatment. Therefore, there is still a need to improve this indicator in the case of Poland.

In the EU, ELT management is organised in the form of material recovery and energy recovery. Pyrolysis of ELTs is a hybrid technology that recovers both materials and energy. Only about 0.5% of ELTs are sent to pyrolysis in the EU, and the process is still only considered an emerging solution (ETRMA, 2021; Verschoor et al., 2021). Given that this method offers great environmental and energy benefits, it should be used to a greater extent than before. This is also a great opportunity for Poland to improve the ELT treatment rate by increasing the share of pyrolysis in ELT management.

ELT pyrolysis is a thermal decomposition process that takes place without air. The primary pyrolysis products are char (33 wt.%), oil (35 wt.%), gas (20 wt.%), and metal (12 wt.%) (Sharma et al., 1998). To improve the cost-effectiveness of this process, pyrolysis gas is usually burned

out to generate energy or to heat the pyrolysis reactor. However, closer inspection revealed that while  $\text{NO}_2$  emissions from waste tyre pyrolysis gas combustion were below the limits set in Waste Incineration Directive (2000), the  $\text{SO}_2$  limit was exceeded by two orders of magnitude (Aylón et al., 2007). The oil is a rich source of compounds from the BTX group and limonene. After desulphurisation, they can be recovered by distillation. After demineralisation and activation, the pyrolysis char can serve as activated carbon and catalyst support. The valorisation of pyrolysis char produces an adsorbent with fairly good adsorption properties that is suitable for adsorption from the gas phase (gas fuel storage, VOC adsorption, adsorption of mercury, mercuric chloride, arsenic, dioxins and furans, and adsorption of  $\text{NO}_x$ ,  $\text{SO}_2$  and  $\text{CO}_2$ ) as well as adsorption from aqueous phase (different inorganic and organic compounds) as shown in previous papers (Kuśmierek et al., 2021a; Kuśmierek et al., 2021b).

Several other important review articles on the pyrolysis of used tyres should also be mentioned, such as (Hoang et al., 2020; Lewandowski et al., 2019; Machin et al., 2017; Martínez et al., 2013; Parthasarathy et al., 2016; Quek and Balasubramanian, 2013; Williams, 2013).

The objective of this work was to investigate the suitability of activated chars from waste tyres as adsorbents for the removal of dyes from water. Synthetic dyes are used in many industries, including rubber and plastics, textiles, cosmet-



ics, pharmaceuticals, paper, and food, among others (Grace Pavithra et al., 2019; Katheresan et al., 2018). The scale of their use is enormous; it is estimated that 100,000 different dyes are produced each year in quantities exceeding 700,000 tons (Katheresan et al., 2018; Rangabhashiyam et al., 2013). In 2021, the estimated global dye market was valued at 33.2 billion USD (Rápó and Tonk, 2021). The consequence of such intensive use of dyes in the industry is a significant increase of water pollution caused by these compounds. Due to the specific nature of dyes, their presence in industrial wastewater and surface water causes several serious consequences. These compounds give colour to water reservoirs, thus deteriorating the aesthetic value of the aquatic ecosystems. Most importantly, however, the presence of dyes in water reduces the penetration of sunlight to aquatic organisms, thereby limiting photosynthesis. Some dyes exhibit toxic properties; in many cases, they have been found to have carcinogenic and mutagenic effects on the human body. Therefore, the presence of colouring compounds in the aquatic ecosystem is undesirable and requires the use of appropriate treatment technologies that can decolorize water and at the same time reduce the toxic effects of dyes according to water quality recommendations and standards (Yagub et al., 2014).

In this work, Rhodamine B (RhB) dye was selected as the model pollutant. The adsorption kinetics and adsorption isotherms as well as the effect of pH on the adsorption efficiency were investigated. As far as the authors know, previous works on RhB adsorption have been carried out on activated tyre pyrolysis chars that have been pre-treated with various chemicals (such as nitric acid, hydrogen peroxide, and toluene) to improve adsorption performance (Li et al., 2010; Saleh and Al-Saadi, 2015) or standardised by grinding and sieving followed by pyrolysis at laboratory conditions (Zhang et al., 2021). Carbon dioxide as an activation agent was used only in the works of Saleh and Al-Saadi (2015) and Zhang et al. (2021), while steam was used by Li et al. (2010). In the present work, tyre pyrolysis char was produced in a pyrolysis pilot plant at conditions more similar to industrial ones. The pyrolysis reactor had a working volume of 75 dm<sup>3</sup> and was fed with 20 kg of ELTs of different types and brands. The obtained tyre pyrolysis char was activated with CO<sub>2</sub> without pre-treatment or standardisation.

## 2. EXPERIMENTAL

### 2.1. Materials

The Rhodamine B dye (RhB) was obtained from Sigma-Aldrich (St. Louis, MO, USA). All other chemicals used in this work were purchased from Chempur (Piekary Śląskie, Poland).

Carbon dioxide (purity  $\geq$  99:99%) delivered by Multax (Poland) was used as purge gas in TGA.

### 2.2. Preparation of activated chars

Tyre pyrolysis char (TPC) was fabricated from shredded ELTs of different types and brands in a pilot plant at the Faculty of Chemical and Process Engineering (Warsaw University of Technology, Poland). The details on the pyrolysis pilot plant can be found elsewhere (Kuśmierk et al., 2020).

About 20 kg of shredded ELT feedstock was fed to a batch tank reactor and pyrolyzed at 773 K under nitrogen. The TPC, oil, and gas yielded 39, 55, and 6 wt.%, respectively. Activated tyre pyrolysis char (AC) was produced from TPC in an electric tube furnace using CO<sub>2</sub>. The activation conditions (temperature and time) were based on our previous thermogravimetric analysis (Kotkowski et al., 2018). These results showed that the carbon burn-off, which occurred as the Boudouard reaction progresses, decreased the yield but simultaneously developed a porous structure of activated char. The maximum BET surface area was observed for the burn-off of about 60% at the constant temperature of 1100 °C. When the burn-off was higher, the fraction of mineral part was too high; thus, the BET surface area decreased (Kotkowski et al., 2018). Taking advantage of these findings, it has been found that mass losses due to the burn-off significantly increased with increasing temperature (in the range of 900–1100 °C) and the contact time of pyrolytic char with CO<sub>2</sub>. This allowed us to select the range of activation times (110–150 min) for the activated pyrolytic chars used in this work. Note also that our activation times were significantly shorter than those used by Zhang et al. (2021), who activated samples for up to 6 h. However, while our activation was carried out at 1100 °C using pure CO<sub>2</sub>, their samples were activated with CO<sub>2</sub> diluted in N<sub>2</sub> (maximum concentration 66 vol.%) at a maximum temperature of 1050 °C.

From the acquired series of samples, a few of the following were selected for further analysis in this work: AC110 (activation time 110 min), AC130 (activation time 130 min), and AC150 (activation time 150 min).

### 2.3. Characterization of the activated chars

The prepared activated tyre pyrolysis chars were characterized using low-temperature nitrogen adsorption analysis. The N<sub>2</sub> adsorption-desorption isotherms were performed on a 3Flex Surface Characterization Analyzer (Micromeritics, USA), at a temperature of 77 K. The specific surface area as well as micro- and mesopore volumes were calculated.

The results of the stereological analysis were shown in our earlier paper (Kotkowski et al., 2020). These previous results showed, for instance, that the most common particle equivalent diameter was in a range of 10–15 µm for both TPC and ATPC. The average particle equivalent diameters were 16.4 ± 14.5 µm and 18.4 ± 16.3 µm for TPC and ATPC, respectively. No significant difference was also found between the TPC and ATPC samples regarding shape factors.

The stereological analysis showed that the grains of TPC and ATPC were quasi-spherical and slightly elongated.

## 2.4. Adsorption study

All adsorption studies were conducted in glass conical flasks into which 20 mL of aqueous RhB solutions of the appropriate concentration and 0.005 g of activated char (adsorbent dose 0.25 g/L) were introduced. The flasks were shaken at 25 °C at a constant speed of 200 rpm. RhB concentrations in the solutions were determined with the UV-Vis spectrophotometry technique (Carry 3E spectrophotometer, Varian, USA). Absorbance measurements were performed at  $\lambda = 553$  nm corresponding to the dye absorption maximum.

The adsorption kinetics was studied for an initial concentration of RhB in a solution equal to 20  $\mu\text{mol/L}$ . The amount of adsorbate that was adsorbed on activated char at time  $t$  ( $q_t$ ,  $\mu\text{mol/g}$ ) was determined using the following relationship:

$$q_t = \frac{(C_0 - C_t)V}{m} \quad (1)$$

A series of solutions with different dye concentrations ranging from 10 to 50  $\mu\text{mol/L}$  (10, 15, 20, 25, 30, 40 and 50  $\mu\text{mol/L}$ ) was used to determine adsorption isotherms. Adsorption at equilibrium ( $q_e$ ,  $\mu\text{mol/g}$ ) was calculated based on Eq. (2):

$$q_e = \frac{(C_0 - C_e)V}{m} \quad (2)$$

The natural (original) pH of the dye solution ( $\sim 5$ ) was selected for the subsequent kinetic and equilibrium studies.

Experiments on the effect of pH on the adsorption of RhB on activated chars were performed in an identical procedure. The initial concentration of the dye was 20  $\mu\text{mol/L}$ ; the pH of the solutions was adjusted to the appropriate level by adding small amounts of NaOH or HCl at a concentration of 0.1 mol/L.

All the adsorption experiments were duplicated, and average values were used for further calculations. The maximum deviation was found to be below 5%.

## 3. RESULTS AND DISCUSSION

### 3.1. Adsorbent characterization

The determined  $\text{N}_2$  adsorption-desorption isotherms for obtained activated tyre pyrolysis chars are presented in Fig. 1.

The calculated specific surface areas as well as micro- and mesopore volumes of the activated tyre pyrolysis chars are given in Table 1 and pore size distributions are shown in Fig. 2.

Parameters of porous structure of obtained activated chars reveal significant differences and are strongly dependent on activation time.

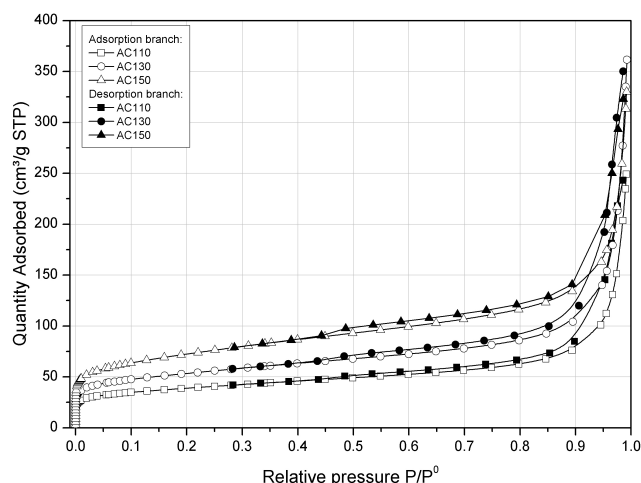


Figure 1. Nitrogen adsorption-desorption isotherms for activated tyre pyrolysis chars at 77 K.

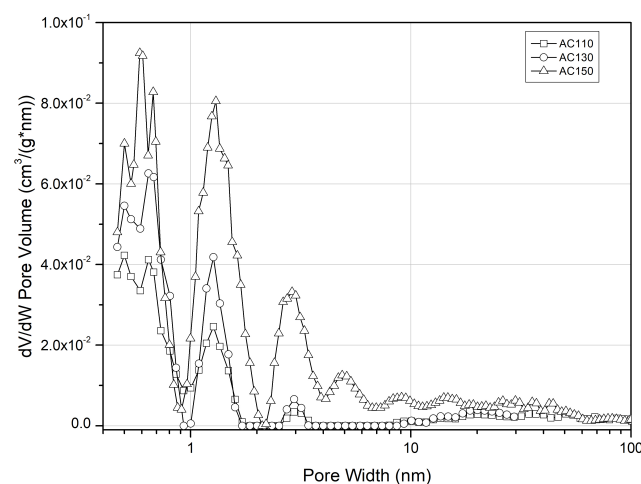


Figure 2. Pore size distributions of the activated char samples.

Table 1. Textural characteristics of the activated chars from waste tyres.

Activated tyre pyrolysis char	$V_t$ [ $\text{cm}^3/\text{g}$ ]	$V_{mi}$ [ $\text{cm}^3/\text{g}$ ]	$V_{me}$ [ $\text{cm}^3/\text{g}$ ]	$S_{\text{BET}}$ [ $\text{m}^2/\text{g}$ ]	C constant
AC110	0.164	0.0627	0.101	138	356
AC130	0.224	0.0864	0.138	191	315
AC150	0.262	0.118	0.144	259	227

### 3.2. Adsorption kinetics

The kinetic curves ( $q_t = f(t)$ ) illustrating the adsorption rate of RhB on activated chars are shown in Fig. 3.

The adsorption equilibrium was established after about 120 min. Two kinetic models, pseudo-first-order and pseudo-second-order (Kajjumba et al., 2018; Tan and Hameed, 2017), were used to describe the obtained experimental data,

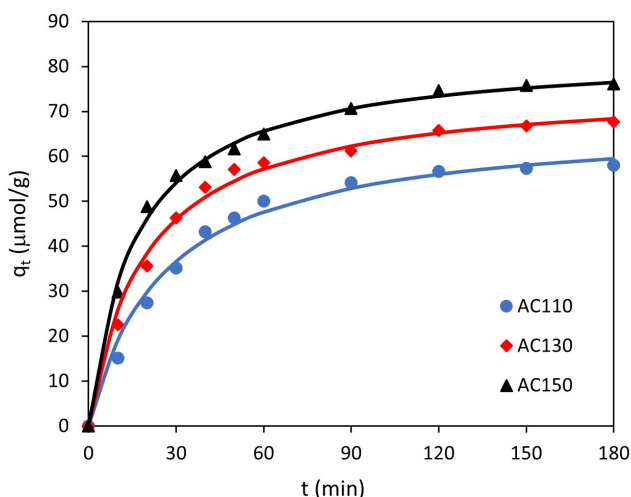


Figure 3. Adsorption kinetics of RhB onto activated chars. Solid lines represent the pseudo-second-order kinetic model (adsorbent dosage = 0.25 g/L, initial RhB concentration = 20  $\mu\text{mol/L}$ , solution pH = original, temperature = 25  $^{\circ}\text{C}$ ).

whose linear forms are expressed by the equations:

$$\log(q_e - q_t) = \log q_e - \frac{k_1}{2.303} t \quad (3)$$

$$\frac{t}{q_t} = \frac{1}{k_2 q_e^2} + \frac{1}{q_e} t \quad (4)$$

The calculated kinetic parameters and the obtained correlation coefficients  $R^2$  are shown in Table 2.

Table 2. Kinetic parameters for the adsorption of RhB onto activated chars.

Kinetic parameter	AC110	AC130	AC150
$q_{\text{exp}}$ [ $\mu\text{mol/g}$ ]	57.96	67.66	76.13
pseudo-first-order			
$q_{\text{cal}}$ [ $\mu\text{mol/g}$ ]	71.41	54.02	87.41
$k_1$ [1/min]	0.040	0.028	0.039
$R^2$	0.913	0.935	0.924
pseudo-second-order			
$q_{\text{cal}}$ [ $\mu\text{mol/g}$ ]	58.03	65.75	73.33
$k_2$ [ $\text{g}/\mu\text{mol}\cdot\text{min}$ ]	$5.47 \times 10^{-4}$	$6.75 \times 10^{-4}$	$7.40 \times 10^{-4}$
$R^2$	0.995	0.998	0.999

By comparing the  $R^2$  values and the agreement of the calculated theoretical  $q_e$  values ( $q_{\text{cal}}$ ) for both models with the experimental  $q_e$  values ( $q_{\text{exp}}$ ), it could be concluded that the adsorption of RhB from water on all activated chars followed a pseudo-second-order model. The kinetic constants  $k_2$  that describe the dye adsorption rate increased in the order: AC110 < AC130 < AC150. This order was due to differences

in the porous structure of the activated chars, especially in the contribution of mesopores to the total pore volume. The AC150 char had the best developed mesoporous structure, which resulted in its best kinetic ability. Mesopores are a kind of "transport pathways" through which RhB molecules enter micropores, where the adsorption process takes place.

Both the pseudo-first-order and pseudo-second-order models do not explain the diffusion of adsorbate into the adsorbent; therefore, to explain the adsorption mechanism as well as the rate-controlling steps (film or intraparticle diffusion) in the adsorption of RhB on the activated chars the Weber-Morris and Boyd kinetic models were used (Kajjumba et al., 2018; Tan and Hameed, 2017).

The Weber-Morris model is given by the following equation:

$$q_t = k_i t^{0.5} + C_i \quad (5)$$

This model assumes that if the relationship  $q_t = f(t^{0.5})$  is a straight-line over the whole range and the curve passes through the origin then adsorption is controlled only by intraparticle diffusion. In contrast, the broken line in the graph (no linearity) indicates that the adsorption processes not only followed intraparticle diffusion but film diffusion also played an important role.

The Boyd equation is given as:

$$\frac{q_t}{q_e} = 1 - \frac{6}{\pi^2} \sum_1^{\infty} \left( \frac{1}{n^2} \right) \exp(-n^2 B_T) \quad (6)$$

where  $B_T$  is a mathematical function of  $q_t/q_e$ .

For the case where  $q_t/q_e < 0.85$ ,  $B_T$  can be expressed as:

$$B_T = \pi \left( 1 - \sqrt{1 - \frac{\pi q_t}{3 q_e}} \right)^2 \quad (7)$$

When  $q_t/q_e > 0.85$ ,  $B_T$  can be calculated by:

$$B_T = -0.4977 - \ln \left( 1 - \frac{q_t}{q_e} \right) \quad (8)$$

The Boyd model assumes that if the plot of  $B_T = f(t)$  is a straight line and passes through the origin, then adsorption is controlled by the intraparticle diffusion step. On the other hand, if the Boyd graph is linear or not linear and does not pass through the origin, then the adsorption rate is controlled by film diffusion.

As shown in Fig. 4, the plots of intraparticle diffusion (Fig. 4a) do not pass through the origin and the curves are all nonlinear while for the Boyd model (Fig. 4b) the curves are all linear and do not pass through the origin. Based on these findings, it can be concluded that for the adsorption of RhB on all the activated chars the film diffusion is a rate-determining step.

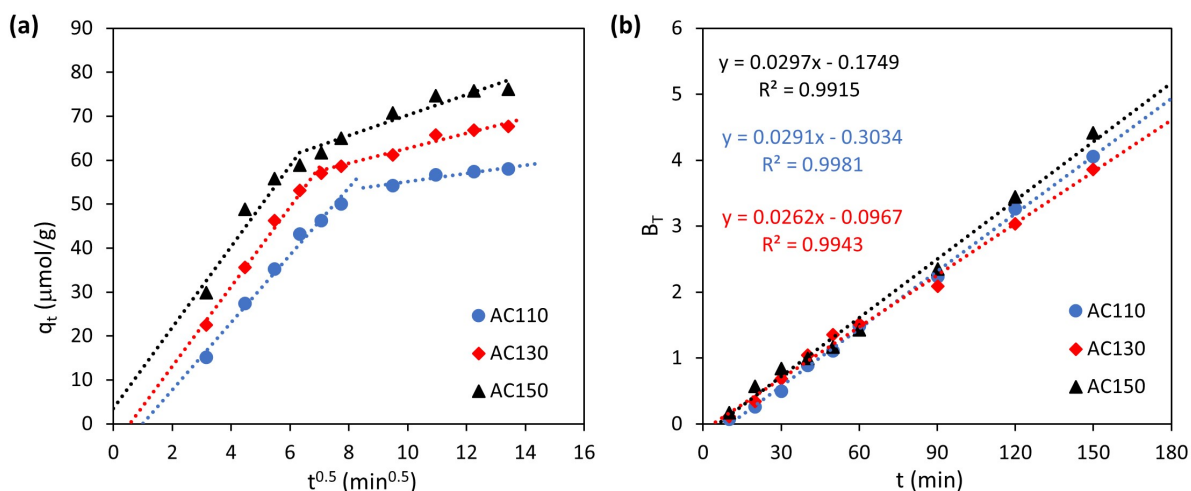


Figure 4. The Weber-Morris model (a), and the plot of Boyd model (b) for the adsorption of RhB on the activated chars.

### 3.3. Adsorption isotherms

The adsorption isotherms of RhB from aqueous solutions on activated chars are shown in Fig. 5.

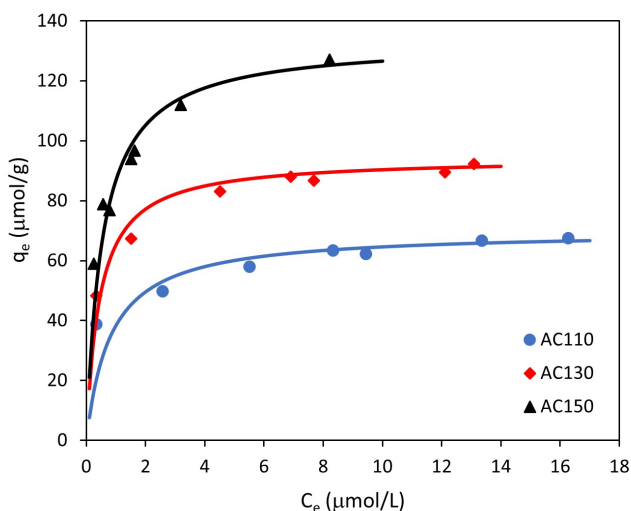


Figure 5. Adsorption isotherms of Rhodamine B on the activated chars. Solid lines represent the Langmuir isotherms (maximum adsorbent dosage = 0.5 g/L, solution pH = original, temperature = 25 °C).

The Langmuir, Freundlich, Temkin, and Elovich isotherm equations were used to describe the experimental data (Al-Ghouti and Da'ana, 2020; Hamdaoui and Naffrechoux, 2007). These equations can be written as:

$$\frac{C_e}{q_e} = \frac{1}{q_{mL}} C_e + \frac{1}{q_{mL} K_L} \quad (9)$$

$$\ln q_e = \ln K_F + \frac{1}{n} \ln C_e \quad (10)$$

$$q_e = \frac{RT}{b_T} \ln A_T + \frac{RT}{b_T} \ln C_e \quad (11)$$

$$\ln \frac{q_e}{C_e} = \ln (K_E q_{mE}) - \frac{1}{q_{mE}} q_e \quad (12)$$

The calculated parameters for all theoretical isotherm models are given in Table 3.

Table 3. Adsorption isotherm parameters for RhB adsorption on the activated chars.

Isotherm	AC110	AC130	AC150
Langmuir			
$q_{mL}$ [µmol/g]	69.93	94.34	133.3
$K_L$ [L/µmol]	1.222	2.253	1.875
$R^2$	0.997	0.996	0.998
Freundlich			
$K_F$ [(µmol/g)(L/µmol) <sup>1/n</sup> ]	44.96	60.02	83.84
$n$	6.757	5.893	4.673
$R^2$	0.988	0.987	0.971
Temkin			
$b_T$ [J·g/(mol·µmol)]	332.0	212.6	128.3
$A_T$ [L/µmol]	394.1	202.3	88.54
$R^2$	0.974	0.988	0.986
Elovich			
$q_{mE}$ [µmol/g]	9.242	14.04	24.81
$K_E$ [L/µmol]	655.8	336.6	107.5
$R^2$	0.968	0.984	0.977

In general, all equations described the adsorption process of RhB on activated chars quite well; nevertheless, the best fit of the applied model to the experimental data was observed for the Langmuir isotherm ( $R^2 \geq 0.996$ ). The good correlation with the Langmuir isotherm model suggests monolayer adsorption with no interactions between the RhB molecules and the homogeneous nature of the adsorbent surface.

RhB was adsorbed the most weakly on AC110, followed by AC130 and preferably on AC150 activated char (AC110 < AC130 < AC150). The monolayer adsorption capacities  $q_{mL}$  calculated from the Langmuir equation were 69.96, 94.34, and 133.3  $\mu\text{mol/g}$  for AC110, AC130, and AC150, respectively. This order was closely correlated with the specific surface area (and activation time) of each activated char as shown in Fig. 6.

A comparison of RhB adsorption on the activated chars used in this work with other activated carbons reported in the literature is presented in Table 4.

The values of maximum Langmuir adsorption capacity ( $q_{mL}$ ) were used for comparison. These values were transformed into the same units (mg/g). In addition, if adsorption studies were conducted under different conditions (e.g. temperature, pH), adsorption capacities obtained under conditions most similar to ours (temp. 25°C, pH ~ 5) were selected for comparison.

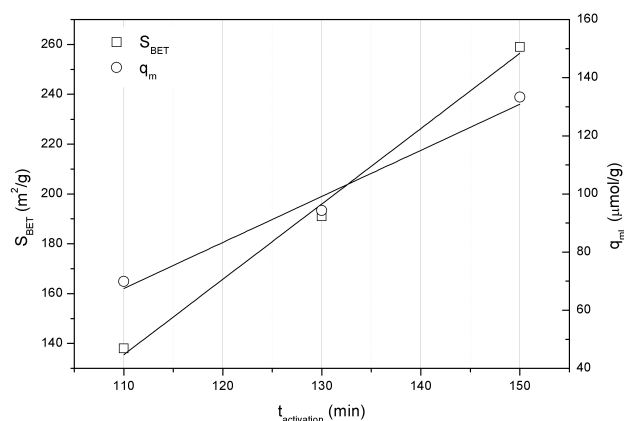


Figure 6. Relationship between activation time, BET surface area, and adsorption capacity.

### 3.4. Effect of pH on RhB adsorption

The pH of the solution is an important parameter that plays a significant role in the adsorption process since pH affects

Table 4. Comparison of adsorption capacities for RhB on various activated carbons.

Adsorbent	Activation agent	S <sub>BET</sub> [m <sup>2</sup> /g]	q <sub>mL</sub> [mg/g]	Ref.
AC from <i>Phragmites australis</i>	H <sub>3</sub> PO <sub>4</sub> /succinic acid	1775	629.7	Guo et al. (2016)
AC from <i>Phragmites australis</i>	H <sub>3</sub> PO <sub>4</sub> /oxalic acid	1040	550.2	Guo et al. (2016)
AC from rice husk	KOH	1803	478.5	Ding et al. (2014)
AC from locust bean husk	H <sub>3</sub> PO <sub>4</sub>	no data	454.5	Bello et al. (2019)
AC from <i>Phragmites australis</i>	H <sub>3</sub> PO <sub>4</sub>	745.7	417.3	Guo et al. (2016)
AC from okra wastes	ZnCl <sub>2</sub>	1044	312.5	Üner et al. (2017)
AC from waste <i>Elaeagnus</i> stone	ZnCl <sub>2</sub>	1588	281.7	Geçgel et al. (2016)
AC from scrap tires	steam (800 °C, 3 h)	720.0	280.1	Li et al. (2010)
AC from bagasse pith	H <sub>3</sub> PO <sub>4</sub>	522.7	263.8	Gad and El-Sayed (2009)
AC from almond shell	H <sub>2</sub> SO <sub>4</sub>	1252	255.4	Abdolrahimi and Tadjarod (2019)
AC from spent tyres	steam (950 °C, 4 h)	667.0	243.0	Zhang et al. (2021)
AC from pericarp of rubber fruit	ZnCl <sub>2</sub>	920.7	110.5	Hayeeye et al. (2014)
AC from palm kernel shell	ZnCl <sub>2</sub>	1365	108.0	Lee and Zaini (2019)
AC150	CO <sub>2</sub>	259.0	63.94	This paper
AC from waste tires	H <sub>2</sub> O <sub>2</sub>	413.0	58.00	Saleh and Al-Saadi (2015)
AC130	CO <sub>2</sub>	191.0	45.21	This paper
AC from carnauba palm	CaCl <sub>2</sub>	430.7	39.22	da Silva Lacerda et al. (2015)
AC from carnauba palm	H <sub>3</sub> PO <sub>4</sub>	402.4	35.28	da Silva Lacerda et al. (2015)
AC from pine nut shell	CaCl <sub>2</sub>	290.1	33.61	da Silva Lacerda et al. (2015)
AC110	CO <sub>2</sub>	138.0	33.52	This paper
AC from macauba seeds	CaCl <sub>2</sub>	265.5	32.96	da Silva Lacerda et al. (2015)
AC from macauba seeds	H <sub>3</sub> PO <sub>4</sub>	371.1	32.65	da Silva Lacerda et al. (2015)
AC from pine nut shell	H <sub>3</sub> PO <sub>4</sub>	296.0	32.50	da Silva Lacerda et al. (2015)
AC from palm shell	CO <sub>2</sub> (900 °C, 3 h)	476.8	1.399	Mohammadi et al. (2010)

the surface charge of the adsorbent as well as the degree of dissociation and the form in which the adsorbate exists in the solution. An important parameter that characterizes the adsorbent and also helps to explain the effect of pH on adsorption is the point of zero charge (pHpzc) which is defined as the pH value at which the surface of the adsorbent is electrically neutral (surface charge of the adsorbent is equal to zero). In a solution at pH below pHpzc, the surface of the adsorbent is positively charged, while in a solution at pH above pHpzc, a negative charge accumulates on the surface of the adsorbent. In this work, pHpzc values of activated chars were determined using the pH drift method and were 7.10, 6.90, and 7.05 for AC110, AC130, and AC150, respectively.

Another important parameter is the  $pK_a$  of the adsorbate, which for RhB equals 3.7. Rhodamine B is a cationic dye, which means that in acidic pH (below  $pK_a$ ) it exists as a positively charged ion ( $RhB^+$ ). At higher pH values (above  $pK_a$ ), due to deprotonation of the carboxyl group, RhB is transformed into a zwitterionic form ( $RhB^\pm$ ). In the case of Rhodamine B, the situation is even more complex, because at higher pH values ( $>pK_a$ ) the dye shows a tendency to aggregate to the dimer form. This is a result of the attractive electrostatic interaction between the carboxyl and xanthene groups of RhB monomers.

In this paper, the effects of solution pH on the adsorption of RhB onto AC110, AC130, and AC150 activated chars were investigated within the pH range of 2.0–10.5 and the results are shown in Fig. 7.

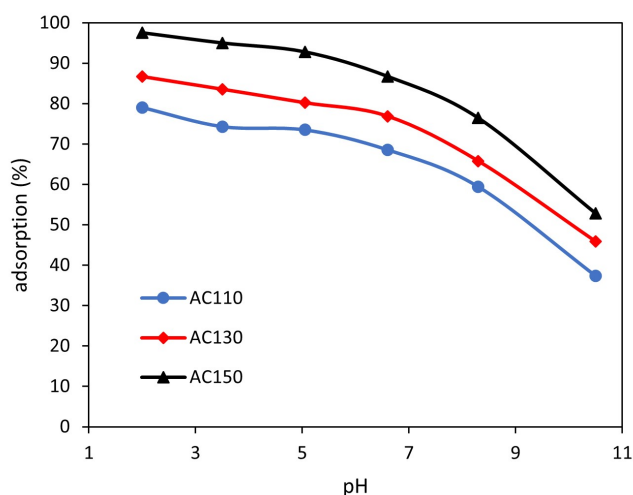


Figure 7. Effect of solution pH on the removal of RhB (adsorbent dosage = 0.25 g/L, initial RhB concentration = 20  $\mu\text{mol/L}$ , temperature = 25  $^\circ\text{C}$ ).

The highest percentage of RhB dye adsorbed was obtained at pH 2.0 and it has been observed that the removal efficiency decreased with an increase of solution pH. When the pH increased from 2.0 to 10.5, RhB adsorption decreased from 79% to 37% for AC110, from 87% to 46% for AC130,

and from 97% to 56% for AC150, respectively. A similar phenomenon (decreasing dye removal efficiency with increasing pH) was observed for RhB adsorption on activated carbons prepared from bagasse pith (Gad and El-Sayed, 2009), rice husk (Ding et al., 2014), locust bean husk (Bello et al., 2019), carnauba palm (da Silva Lacerda et al., 2015), macauba seeds (da Silva Lacerda et al., 2015), pine nut-shell (da Silva Lacerda et al., 2015), zeolite modified with graphene oxide (Yu et al., 2013), rice husk (Jain et al., 2007), and halloysites (Wierzbicka et al., 2022).

As reported by Dutta et al. (2021), dye adsorption is very complex and can take place *via* electrostatic attraction,  $\pi$ - $\pi$  interactions, van der Waals forces, hydrogen bonding, and hydrophobic interactions. According to Yu et al. (2013), in an acidic environment ( $\text{pH} < pK_a$  and pHpzc), RhB can interact with the adsorbent surface through electrostatic, hydrophobic, and hydrogen bonding interactions, while at higher pH ( $\text{pH} > pK_a$  and pHpzc) the dye can be adsorbed due to attractive and repulsive electrostatic interactions as well as hydrogen bonding interactions. The results shown in Fig. 7 indicate first that the percentage of dye removal strongly depends on the pH of the solution. Second, the maximum adsorption of RhB on all the activated chars was recorded at pH 2.0, at which the dye molecules are in cationic and monomeric form and the adsorbent surface is positively charged. A similar finding was reported by Jain and collaborators (Jain et al., 2007) who explained this phenomenon by increasing the protonation of the adsorbent which generated more active sites on the surface of the adsorbent, thus increasing the surface adsorption. The results suggest that in this case, adsorption takes place due mainly to hydrophobic interactions and/or hydrogen bonds between the dye molecules and the adsorbent surface rather than owing to electrostatic interactions.

As can be seen in Fig. 7, when the pH of the solution increased, adsorption decreased. At higher pH, the RhB existed in zwitterionic form and the surface of the adsorbent was negatively charged. Thus, the lower percentage of RhB removal may be due in part to the repulsive electrostatic interactions between the negatively charged surface of the adsorbent and negative hydroxyl ions in the dye molecules. The negatively charged surface of the adsorbent could, nevertheless, at least theoretically, interact with the positive charges located in the dye molecule. Such attractive electrostatic interactions could increase adsorption efficiency. However, the results show the opposite effect. Therefore, it seems that also at higher pH values adsorbate-adsorbent electrostatic interactions play a secondary role.

The effect of pH on Rhodamine B adsorption observed in Fig. 7 may be related to the form (monomeric or dimeric) in which the dye can exist in the solution. Adsorption is promoted in an acidic environment because smaller monomeric RhB occurring at  $\text{pH} < pK_a$  can easily diffuse into the micropores of the adsorbent. In contrast, a larger molecular form

(dimer) of the dye occurring at  $\text{pH} > \text{pK}_a$  is unable to enter the micropores as a result of their size thereby resulting in a decrease in adsorption at higher pH.

## 4. CONCLUSIONS

In previous works of other authors on the adsorption of RhB from water on activated chars from tyre pyrolysis, nonactivated precursors were pre-treated with various chemical compounds to improve adsorption performance or standardised by grinding and sieving followed by repeated pyrolysis under laboratory conditions. On the other hand, our nonactivated precursor was produced in a pyrolysis pilot plant under conditions similar to industrial ones, without further char treatment or standardisation. The pyrolysis reactor had a working capacity of  $75 \text{ dm}^3$  and was fed with 20 kg ELTs of various types and brands. Unlike in these previous works of other authors, our nonactivated pyrolysis char was activated with pure  $\text{CO}_2$  at the activation temperature and times that were selected based on prior TGA.

In this paper, batch adsorption experiments were carried out for the removal of Rhodamine B dye from the aqueous solution using activated chars from end-of-life tyre pyrolysis varying in the activation time (AC110 – 110 min, AC130 – 130 min, and AC150 – 150 min). The results showed that the adsorption of dye was pH-dependent and decreased with the increasing pH of the solution. The data were best fitted to the pseudo-second-order kinetic model as well as the Langmuir isotherm model. RhB was adsorbed the most weakly on AC110, followed by AC130 and preferably on AC150 activated char ( $\text{AC110} < \text{AC130} < \text{AC150}$ ). This order was closely correlated with the specific surface area (and activation time) of each activated char.

## SYMBOLS

$A_T$	Temkin isotherm constants, $\text{L}/\mu\text{mol}$
$b_T$	Temkin constant related to adsorption heat, $\text{J}\cdot\text{g}/(\text{mol}\cdot\mu\text{mol})$
$B_T$	mathematical function of $q_t/q_e$
C–BET	C–BET constant
$C_0$	initial concentration of RhB, $\mu\text{mol}/\text{L}$
$C_e$	equilibrium concentration of RhB in solution, $\mu\text{mol}/\text{L}$
$C_i$	parameter of the Weber-Morris model correlated with the thickness of the boundary layer, $\mu\text{mol}/\text{g}$
$C_t$	concentration of RhB after time $t$ , $\mu\text{mol}/\text{L}$
$k_1$	adsorption rate constant of the pseudo-first-order adsorption, $1/\text{min}$
$k_2$	adsorption rate constant of the pseudo-second-order adsorption, $\text{g}/\mu\text{mol}\cdot\text{min}$
$K_E$	Elovich equilibrium constant, $\text{L}/\mu\text{mol}$
$K_F$	Freundlich isotherm constant, $(\mu\text{mol}/\text{g})(\text{L}/\mu\text{mol})^{1/n}$

$k_i$	intraparticle diffusion rate constant, $\mu\text{mol}/\text{g}\cdot\text{min}^{0.5}$
$K_L$	Langmuir isotherm constant, $\text{L}/\mu\text{mol}$
$m$	mass of the adsorbent, g
$n$	Freundlich isotherm constants
$q_{\text{cal}}$	adsorption capacity model-predicted value, $\mu\text{mol}/\text{g}$
$q_e$	adsorption capacity at equilibrium, $\mu\text{mol}/\text{g}$
$q_{\text{exp}}$	experimental adsorption capacity, $\mu\text{mol}/\text{g}$
$q_{mE}$	Elovich maximum adsorption capacity, $\mu\text{mol}/\text{g}$
$q_{mL}$	Langmuir maximum adsorption capacity, $\mu\text{mol}/\text{g}$ or $\text{mg}/\text{g}$
$q_t$	adsorption capacity at time $t$ , $\mu\text{mol}/\text{g}$
$R$	universal gas constant, $8.314 \text{ J}/\text{mol}\cdot\text{K}$
$R^2$	correlation coefficient
$S_{\text{BET}}$	specific surface area, $\text{m}^2/\text{g}$
$t$	time, min
$t_{\text{activation}}$	activation time, min
$T$	temperature, K
$V$	volume of the solution, L
$V_{me}$	mesopore volume, $\text{cm}^3/\text{g}$
$V_{mi}$	micropore volume, $\text{cm}^3/\text{g}$
$V_t$	total pore volume, $\text{cm}^3/\text{g}$

## REFERENCES

- Abdolrahimi N., Tadjard A., 2019. Adsorption of Rhodamine-B from aqueous solution by activated carbon from almond shell. *Proceedings*, 41(1), 51. DOI: [10.3390/ecsoc-23-06619](https://doi.org/10.3390/ecsoc-23-06619).
- Al-Ghouti M.A., Da'ana D.A., 2020. Guidelines for the use and interpretation of adsorption isotherm models: A review. *J. Hazard. Mater.*, 393, 122383. DOI: [10.1016/j.jhazmat.2020.122383](https://doi.org/10.1016/j.jhazmat.2020.122383).
- Aylón E., Murillo R., Fernández-Colino A., Aranda A., García T., Callén M.S., Mastral A.M., 2007. Emissions from the combustion of gas-phase products at tyre pyrolysis. *J. Anal. Appl. Pyrolysis*, 79, 210–214. DOI: [10.1016/j.jaap.2006.10.009](https://doi.org/10.1016/j.jaap.2006.10.009).
- Bello O.S., Adegoke K.A., Sarumi O.O., Lameed O.S., 2019. Functionalized locust bean pod (*Parkia biglobosa*) activated carbon for Rhodamine B dye removal. *Heliyon*, 5, e02323. DOI: [10.1016/j.heliyon.2019.e02323](https://doi.org/10.1016/j.heliyon.2019.e02323).
- da Silva Lacerda V., López-Sotelo J.B., Correa-Guimarães A., Hernández-Navarro S., Sánchez-Báscones M., Navas-Gracia L.M., Martín-Ramos P., Martín-Gil J., 2015. Rhodamine B removal with activated carbons obtained from lignocellulosic waste. *J. Environ. Manage.*, 155, 67–76. DOI: [10.1016/j.jenvman.2015.03.007](https://doi.org/10.1016/j.jenvman.2015.03.007).
- Ding L., Zou B., Gao W., Liu Q., Wang Z., Guo Y., Wang X., Liu X., 2014. Adsorption of Rhodamine-B from aqueous solution using treated rice husk-based activated carbon. *Colloids Surf. A*, 446, 1–7. DOI: [10.1016/j.colsurfa.2014.01.030](https://doi.org/10.1016/j.colsurfa.2014.01.030).
- Directive 2000/76/EC of the European Parliament and of the Council of 4 December 2000 on the incineration of waste. *OJ L* 332, 28.12.2000, 91–111.
- Dutta S., Gupta B., Srivastava S.K., Gupta A.K., 2021. Recent advances on the removal of dyes from wastewater using various

- adsorbents: a critical review. *Mater. Adv.*, 2, 4497–4531. DOI: [10.1039/d1ma00354b](https://doi.org/10.1039/d1ma00354b).
- ETRMA-European Tyre and Rubber Manufacturers' Association, 2021. In Europe 95% of all End of Life Tyres were collected and treated in 2019. Available at: [https://www.etrma.org/wp-content/uploads/2021/05/20210520\\_ETRMA\\_PRESS\\_REL\\_EASE\\_ELT-2019.pdf](https://www.etrma.org/wp-content/uploads/2021/05/20210520_ETRMA_PRESS_REL_EASE_ELT-2019.pdf).
- Gad H.M.H., El-Sayed A.A., 2009. Activated carbon from agricultural by-products for the removal of Rhodamine-B from aqueous solution. *J. Hazard. Mater.*, 168, 1070–1081. DOI: [10.1016/j.jhazmat.2009.02.155](https://doi.org/10.1016/j.jhazmat.2009.02.155).
- Geçgel Ü., Üner O., Gökara G., Bayrak Y., 2016. Adsorption of cationic dyes on activated carbon obtained from waste *Elaeagnus* stone. *Adsorpt. Sci. Technol.*, 34(9-10), 512–525. DOI: [10.1177/0263617416669727](https://doi.org/10.1177/0263617416669727).
- Grace Pavithra K., Senthil Kumar P., Jaikumar V., Sundar Rajan P., 2019. Removal of colorants from wastewater: A review on sources and treatment strategies. *J. Ind. Eng. Chem.*, 75, 1–19. DOI: [10.1016/j.jiec.2019.02.011](https://doi.org/10.1016/j.jiec.2019.02.011).
- Guo Z., Zhang J., Liu H., 2016. Ultra-high Rhodamine B adsorption capacities from an aqueous solution by activated carbon derived from *Phragmites australis* doped with organic acid by phosphoric acid activation. *RSC Adv.*, 6, 40818–40827. DOI: [10.1039/c5ra25200h](https://doi.org/10.1039/c5ra25200h).
- Hamdaoui O., Naffrechoux E., 2007. Modeling of adsorption isotherms of phenol and chlorophenols onto granular activated carbon Part I. Two-parameter models and equations allowing determination of thermodynamic parameters. *J. Hazard. Mater.*, 147, 381–394. DOI: [10.1016/j.jhazmat.2007.01.021](https://doi.org/10.1016/j.jhazmat.2007.01.021).
- Hayeeye F., Sattar M., Tekasakul S., Sirichote O., 2014. Adsorption of Rhodamine B on activated carbon obtained from pericarp of rubber fruit in comparison with the commercial activated carbon. *Songklanakarın J. Sci. Technol.*, 36(2), 177–187.
- Hoang A.T., Nguyen T.H., Nguyen H.P., 2020. Scrap tire pyrolysis as a potential strategy for waste management pathway: a review. *Energy Sources, Part A Recover. Util. Environ. Eff.* 00, 1–18. DOI: [10.1080/15567036.2020.1745336](https://doi.org/10.1080/15567036.2020.1745336).
- Jain R., Mathur M., Sikarwar S., Mittal A., 2007. Removal of the hazardous dye rhodamine B through photocatalytic and adsorption treatments. *J. Environ. Manage.*, 85, 956–964. DOI: [10.1016/j.jenvman.2006.11.002](https://doi.org/10.1016/j.jenvman.2006.11.002).
- Kajjumba G.W., Emik S., Öngen A., Özcan H.K., Aydın S., 2018. Modelling of adsorption kinetic processes – errors, theory and application, In: Edebalı S. (Ed.), *Advanced Sorption Process Applications*. IntechOpen Limited, Rijeka, 1-19. DOI: [10.5772/intechopen.80495](https://doi.org/10.5772/intechopen.80495).
- Katheresan V., Kansedo J., Lau S.Y., 2018. Efficiency of various recent wastewater dye removal methods: A review. *J. Environ. Chem. Eng.*, 6, 4676–4697. DOI: [10.1016/j.jece.2018.06.060](https://doi.org/10.1016/j.jece.2018.06.060).
- Kotkowski T., Cherbański R., Molga E., 2018. Acetone adsorption on CO<sub>2</sub>-activated tyre pyrolysis char – Thermogravimetric analysis. *Chem. Process Eng.*, 39, 233–246. DOI: [10.24425/122946](https://doi.org/10.24425/122946).
- Kotkowski T.P., Cherbański R., Molga E., 2020. Tyre-derived activated carbon – textural properties and modelling of adsorption equilibrium of n-hexane. *Chem. Process Eng.*, 41, 25–44. DOI: [10.24425/cpe.2019.130221](https://doi.org/10.24425/cpe.2019.130221).
- Kuśmierk K., Świątkowski A., Kotkowski T., Cherbański R., Molga E., 2021a. Adsorption on activated carbons from end-of-life tyre pyrolysis for environmental applications. Part I. preparation of adsorbent and adsorption from gas phase. *J. Anal. Appl. Pyrolysis*, 157, 105205. DOI: [10.1016/j.jaap.2021.105205](https://doi.org/10.1016/j.jaap.2021.105205).
- Kuśmierk K., Świątkowski A., Kotkowski T., Cherbański R., Molga E., 2021b. Adsorption on activated carbons from end-of-life tyre pyrolysis for environmental applications. Part II. Adsorption from aqueous phase. *J. Anal. Appl. Pyrolysis*, 158, 105206. DOI: [10.1016/j.jaap.2021.105206](https://doi.org/10.1016/j.jaap.2021.105206).
- Kuśmierk K., Świątkowski A., Kotkowski T., Cherbański R., Molga E., 2020. Adsorption properties of activated tire pyrolysis chars for phenol and chlorophenols. *Chem. Eng. Technol.*, 43, 770–780. DOI: [10.1002/ceat.201900574](https://doi.org/10.1002/ceat.201900574).
- Lee L.Z, Zaini M.A.A., 2019. Rhodamine B dyes adsorption on palm kernel shell based activated carbons. *Malays. J. Fund. Appl. Sci.*, 15(5), 743–747.
- Lewandowski W.M., Januszewicz K., Kosakowski W., 2019. Efficiency and proportions of waste tyre pyrolysis products depending on the reactor type – A review. *J. Anal. Appl. Pyrolysis*, 140, 25–53. DOI: [10.1016/j.jaap.2019.03.018](https://doi.org/10.1016/j.jaap.2019.03.018).
- Li L., Liu S., Zhu T., 2010. Application of activated carbon derived from scrap tires for adsorption of Rhodamine B. *J. Environ. Sci.*, 22(8), 1273–1280. DOI: [10.1016/S1001-0742\(09\)60250-3](https://doi.org/10.1016/S1001-0742(09)60250-3).
- Machin E.B., Pedroso D.T., de Carvalho J.A., 2017. Energetic valorization of waste tires. *Renewable Sustainable Energy Rev.*, 68, 306–315. DOI: [10.1016/j.rser.2016.09.110](https://doi.org/10.1016/j.rser.2016.09.110).
- Martínez J.D., Puy N., Murillo R., García T., Navarro M.V., Mastral A.M., 2013. Waste tyre pyrolysis – A review. *Renewable Sustainable Energy Rev.*, 23, 179–213. DOI: [10.1016/j.rser.2013.02.038](https://doi.org/10.1016/j.rser.2013.02.038).
- Mohammadi M., Hassani A.J., Mohamed A.R., Najafpour G.D., 2010. Removal of Rhodamine B from aqueous solution using palm shell-based activated carbon: adsorption and kinetic studies. *J. Chem. Eng. Data*, 55, 5777–5785. DOI: [10.1021/je100730a](https://doi.org/10.1021/je100730a).
- Parthasarathy P., Choi H.S., Park H.C., Hwang J.G., Yoo H.S., Lee B.K., Upadhyay M., 2016. Influence of process conditions on product yield of waste tyre pyrolysis – A review. *Korean J. Chem. Eng.*, 33, 2268–2286. DOI: [10.1007/s11814-016-0126-2](https://doi.org/10.1007/s11814-016-0126-2).
- Quek A., Balasubramanian R., 2013. Liquefaction of waste tires by pyrolysis for oil and chemicals – A review. *J. Anal. Appl. Pyrolysis*, 101, 1–16. DOI: [10.1016/j.jaap.2013.02.016](https://doi.org/10.1016/j.jaap.2013.02.016).
- Rangabhashiyam S., Anu N., Selvaraju N., 2013. Sequestration of dye from textile industry wastewater using agricultural waste products as adsorbents. *J. Environ. Chem. Eng.*, 1, 629–641. DOI: [10.1016/j.jece.2013.07.014](https://doi.org/10.1016/j.jece.2013.07.014).
- Rápó E., Tonk, S., 2021. Factors affecting synthetic dye adsorption; desorption studies: A review of results from the last five years (2017–2021). *Molecules*, 26, 5419. DOI: [10.3390/molecules26175419](https://doi.org/10.3390/molecules26175419).
- Saleh T.A., Al-Saadi A.A., 2015. Surface characterization and sorption efficacy of tire-obtained carbon: experimental and semiempirical study of rhodamine B adsorption. *Surf. Interface Anal.*, 2015, 47, 785–792. DOI: [10.1002/sia.5775](https://doi.org/10.1002/sia.5775).

- Sharma V.K., Mincarini M., Fortuna F., Cognini F., Cornacchia G., 1998. Disposal of waste tyres for energy recovery and safe environment – Review. *Energy Convers. Manage.*, 39, 511–528. DOI: [10.1016/S0196-8904\(97\)00044-7](https://doi.org/10.1016/S0196-8904(97)00044-7).
- Tan K.L., Hameed B.H., 2017. Insight into the adsorption kinetics models for the removal of contaminants from aqueous solutions. *J. Taiwan Inst. Chem. Eng.*, 74, 25–48. DOI: [10.1016/j.jtice.2017.01.024](https://doi.org/10.1016/j.jtice.2017.01.024).
- Üner O., Geçgel Ü., Kolancılar H., Bayrak Y., 2017. Adsorptive removal of Rhodamine B with activated carbon obtained from okra wastes. *Chem. Eng. Commun.*, 204(7), 772–783. DOI: [10.1080/00986445.2017.1319361](https://doi.org/10.1080/00986445.2017.1319361).
- Verschoor A.J., van Gelderen A., Hofstra U., 2021. Fate of recycled tyre granulate used on artificial turf. *Environ. Sci. Eur.*, 33, 27. DOI: [10.1186/s12302-021-00459-1](https://doi.org/10.1186/s12302-021-00459-1).
- Wierzbicka E., Kuśmierek K., Świątkowski A., Legocka I., 2022. Efficient Rhodamine B dye removal from water by acid- and organo-modified halloysites. *Minerals*, 12(3), 350. DOI: [10.3390/min12030350](https://doi.org/10.3390/min12030350).
- Williams P.T., 2013. Pyrolysis of waste tyres: A review. *Waste Manage.*, 33, 1714–1728. DOI: [10.1016/j.wasman.2013.05.003](https://doi.org/10.1016/j.wasman.2013.05.003).
- Yagub M.T., Sen T.K., Afroze S., Ang H.M., 2014. Dye and its removal from aqueous solution by adsorption: A review. *Adv. Colloid Interface Sci.*, 209, 172–184. DOI: [10.1016/j.cis.2014.04.002](https://doi.org/10.1016/j.cis.2014.04.002).
- Yu Y., Murthy B.N., Shapter J.G., Constantopoulos K.T., Voelcker N.H., Ellis A.V., 2013. Benzene carboxylic acid derivatized graphene oxide nanosheets on natural zeolites as effective adsorbents for cationic dye removal. *J. Hazard. Mater.*, 260, 330–338. DOI: [10.1016/j.jhazmat.2013.05.041](https://doi.org/10.1016/j.jhazmat.2013.05.041).
- Zhang J., Zhu M., Jones I., Zhang Z., Gao J., Zhang D., 2021. Performance of activated carbons prepared from spent tyres in the adsorption of rhodamine B in aqueous solutions. *Environ. Sci. Pollut. Res.*, 28, 52862–52872. DOI: [10.1007/s11356-021-14502-4](https://doi.org/10.1007/s11356-021-14502-4).